Supercontinuum generation in a high index doped silica glass spiral waveguide

David Duchesne[1], Marco Peccianti[1,2], Michael R. E. Lamont[1,3], Marcello Ferrera[1], Luca Razzari[1,4], Francois Légaré[1], Roberto Morandotti[1], Sai Chu[5], Brent E. Little[5] and David J. Moss[1,3,*]

[1]INRS-EMT, 1650 Boulevard Lionel Boulet, Varennes, Québec J3X 1S2, Canada
[2]Research Center SOFT INFM-CNR, "Sapienza" University, P. A. Moro 2, 00185 Rome, Italy
[3]CUDOS, School of Physics, University of Sydney, New South Wales 2006, Australia
[4] Dept of Electronics., University of di Pavia, Via Ferrata 1, 27100 Pavia, Italy
[5]Infinera Corp, 9020 Junction Drive, Annapolis, Maryland 94089, USA
**dmoss@physics.usyd.edu.au*

Abstract: We demonstrate supercontinuum (SC) generation at both 1550 nm and 1288 nm in a compact (< 5mm^2) 45 cm spiral waveguide composed of CMOS-compatible doped high-index glass. While both wavelengths have weak dispersion and are near zero dispersion points, they present different symmetries. At 1550nm, the normal dispersion regime takes place at longer wavelengths, whereas at 1290nm it is at shorter wavelengths, and we observe features in the SC spectra that clearly reflect this. In particular, the spectrum at 1550 nm is more than 300 nm wide (limited by detection) and is well reproduced by simulations based on the measured dispersion. This work represents a practical on-chip broadband wavelength source with potential use in many important applications.

OCIS codes: (320.6629) Supercontinuum generation; (130.2755) Glass waveguides; (160.4330) Nonlinear optical materials; (190.3270) Integrated optics materials

References and links

1. J. M. Dudley, G. Genty, and S. Coen, "Supercontinuum generation in photonic crystal fiber," Rev. Mod. Phys. **78**(4), 1135–1184 (2006).
2. M. H. Frosz, T. Sorensen, and O. Bang, "Nanoengineering of photonic crystal fibers for supercontinuum spectral shaping," J. Opt. Soc. Am. B **23**(8), 1692–1699 (2006).
3. T. A. Birks, W. J. Wadsworth, and P. S. Russell, "Supercontinuum generation in tapered fibers," Opt. Lett. **25**(19), 1415–1417 (2000).
4. C. M. B. Cordeiro, W. J. Wadsworth, T. A. Birks, and P. S. J. Russell, "Engineering the dispersion of tapered fibers for supercontinuum generation with a 1064 nm pump laser," Opt. Lett. **30**(15), 1980–1982 (2005).
5. R. R. Gattass, G. T. Svacha, L. M. Tong, and E. Mazur, "Supercontinuum generation in submicrometer diameter silica fibers," Opt. Express **14**(20), 9408–9414 (2006).
6. S. G. Leon-Saval, T. A. Birks, W. J. Wadsworth, P. St. J. Russell, and M. W. Mason, "Supercontinuum generation in submicron fibre waveguides," Opt. Express **12**(13), 2864 (2004).
7. J. Y. Y. Leong, P. Petropoulos, J. H. V. Price, H. Ebendorff-Heidepriem, S. Asimakis, R. C. Moore, K. E. Frampton, V. Finazzi, X. Feng, T. M. Monro, and D. J. Richardson, "High-nonlinearity dispersion-shifted lead-silicate holey fibers for efficient 1-μm pumped supercontinuum generation," J. Lightwave Technol. **24**(1), 183–190 (2006).
8. J. H. V. Price, T. M. Monro, H. Ebendorff-Heidepriem, F. Poletti, V. Finazzi, J. Y. Y. Leong, P. Petropoulos, J. C. Flanagan, G. Brambilla, X. Feng, and D. J. Richardson, "Non-silica microstructured optical fibers for mid-IR supercontinuum generation from 2 μm - 5 μm," Proc. SPIE **6102**, 54–68 (2006).
9. G. Brambilla, F. Koizumi, V. Finazzi, and D. J. Richardson, "Supercontinuum generation in tapered bismuth silicate fibres," Electron. Lett. **41**(14), 795–797 (2005).
10. D.-I. Yeom, E. C. Mägi, M. R. E. Lamont, M. A. F. Roelens, L. Fu, and B. J. Eggleton, "Low-threshold supercontinuum generation in highly nonlinear chalcogenide nanowires," Opt. Lett. **33**(7), 660–662 (2008).
11. I. W. Hsieh, X. G. Chen, X. P. Liu, J. I. Dadap, N. C. Panoiu, C. Y. Chou, F. N. Xia, W. M. Green, Y. A. Vlasov, and R. M. Osgood, "Supercontinuum generation in silicon photonic wires," Opt. Express **15**(23), 15242–15249 (2007).
12. L. H. Yin, Q. Lin, and G. P. Agrawal, "Soliton fission and supercontinuum generation in silicon waveguides," Opt. Lett. **32**(4), 391–393 (2007).

#120004 - $15.00 USD Received 16 Nov 2009; revised 19 Dec 2009; accepted 20 Dec 2009; published 6 Jan 2010

13. M. R. E. Lamont, B. Luther-Davies, D.-Y. Choi, S. Madden, and B. J. Eggleton, "Supercontinuum generation in dispersion engineered highly nonlinear (γ = 10 /W/m) As_2S_3) chalcogenide planar waveguide," Opt. Express **16**(19), 14938–14944 (2008).
14. A. D. Bristow, N. Rotenberg, and H. M. van Driel, "Two-photon absorption and Kerr coefficients of silicon for 850–2200 nm," Appl. Phys. Lett. **90**(19), 191104 (2007).
15. P. V. Koonath, D. R. Solli, and B. Jalali, "Limiting Nature of Continuum Generation in Silicon," in *Conference on Lasers and Electro-Optics/Quantum Electronics and Laser Science Conference and Photonic Applications Systems Technologies*, Optical Society of America, CFC4 (2008).
16. B. J. Eggleton, D. J. Moss, and S. Radic, "Nonlinear Optics in Communications: From Crippling Impairment to Ultrafast Tools," (Academic Press, Oxford, 2008).
17. K. Ikeda, R. E. Saperstein, N. Alic, and Y. Fainman, "Thermal and Kerr nonlinear properties of plasma-deposited silicon nitride/ silicon dioxide waveguides," Opt. Express **16**(17), 12987–12994 (2008).
18. J. S. Levy, A. Gondarenko, A. C. Turner-Foster, M. A. Foster, A. L. Gaeta, and M. Lipson, "Four-wave Mixing in Integrated Silicon Nitride Waveguides", Paper CMFF5, Conference for Lasers and Electro Optics (CLEO), Baltimore MA, May (2009).
19. D. Duchesne, M. Ferrera, L. Razzari, R. Morandotti, B. E. Little, S. T. Chu, and D. J. Moss, "Efficient self-phase modulation in low loss, high index doped silica glass integrated waveguides," Opt. Express **17**(3), 1865–1870 (2009).
20. B. E. Little, "A VLSI photonics platform," in *Conference on Optical Fiber Communication (OFC)*, 444–445 (2003).
21. A. Yalcin, K. C. Popat, J. C. Aldridge, T. A. Desai, J. Hryniewicz, N. Chbouki, B. E. Little, O. King, V. Van, S. Chu, D. Gill, M. Anthes-Washburn, and M. S. Unlu, "Optical sensing of biomolecules using microring resonators," IEEE J. Sel. Top. Quantum Electron. **12**(1), 148–155 (2006).
22. B. E. Little, S. T. Chu, P. P. Absil, J. V. Hryniewicz, F. G. Johnson, E. Seiferth, D. Gill, V. Van, O. King, and M. Trakalo, "Very high-order microring resonator filters for WDM applications," IEEE Photon. Technol. Lett. **16**(10), 2263–2265 (2004).
23. M. Ferrera, D. Duchesne, L. Razzari, M. Peccianti, R. Morandotti, P. Cheben, S. Janz, D. X. Xu, B. E. Little, S. Chu, and D. J. Moss, "Low power four wave mixing in an integrated, micro-ring resonator with Q=1.2 million," Opt. Express **17**(16), 14098–14103 (2009).
24. M. Ferrera, L. Razzari, D. Duchesne, R. Morandotti, Z. Yang, M. Liscidini, J. E. Sipe, S. Chu, B. E. Little, and D. J. Moss, "Low-power continuous-wave nonlinear optics in doped silica glass integrated waveguide structures," Nat. Photonics **2**(12), 737–740 (2008).
25. L. Razzari, D. Duchesne, M. Ferrera, R. Morandotti, B. E. Little, S. Chu, and D. J. Moss, "CMOS compatible integrated optical hyper-parametric oscillator," Nature Photon. doi: 10.1038/NPHOTON.2009.236.
26. M. R. E. Lamont, B. T. Kuhlmey, and C. M. de Sterke, "Multi-order dispersion engineering for optimal four-wave mixing," Opt. Express **16**(10), 7551–7563 (2008).
27. G. P. Agrawal, *Nonlinear Fiber Optics,* 3rd ed., Quantum electronics - principles and applications (Academic Press, San Diego, California, 2001).

1. Introduction

Supercontinuum (SC) generation describes the creation of ultra-broadband spectra using spectrally narrow pulses, and has applications to multi-wavelength and tunable sources, spectroscopy, bio-imaging, pulse compression, optical coherence tomography and many others (see [1] and references therein). In particular, an integrated SC source would be invaluable for modern wavelength-division multiplexing (WDM) systems, where a single laser employed with spectral filters could replace several laser sources, thereby reducing costs, complexity and size. On a more fundamental level, SC generation is of interest to researchers in nonlinear optics since it involves a rich tapestry of many different processes, such as self-phase modulation (SPM), cross-phase modulation (XPM), four-wave mixing (FWM), soliton fission, Raman self-frequency shift (SFS), and the generation of Cherenkov radiation [1]. Much of this research has traditionally been performed in silica photonic crystal fibers (PCFs) [1, 2] and tapered fibers [3–6]. To achieve SC generation in shorter lengths and lower powers, nonlinear glasses have also been used in PCFs [7, 8] and in fiber tapers [9, 10].

More recently, on-chip SC generation has been reported [11–13], which can potentially lead to integrated devices with compact footprints for low-cost mass-production. Silicon waveguides have a very high nonlinear index (n_2 = 5 x 10^{-14} cm^2/W [14]), however they also have relatively high linear losses (compared with glass) and nonlinear losses, characterized by intrinsic two-photon absorption and the subsequently induced free carrier absorption, both of which limit the spectral broadening [15]. Chalcogenide glass waveguides, such as As_2S_3, also have a high n_2 (n_2 = 3 x 10^{-14} cm^2/W [16]) while exhibiting very low two-photon absorption. Recently, silicon nitride has also been shown to be a promising platform for nonlinear optics

#120004 - $15.00 USD Received 16 Nov 2009; revised 19 Dec 2009; accepted 20 Dec 2009; published 6 Jan 2010

[17, 18], with an n_2 approximately ten times larger than in silica glass and an index contrast of 25%.

In this paper, we demonstrate SC generation in a 45cm long high-index doped silica glass spiral waveguide. Our waveguide core has a Kerr nonlinearity approximately five times higher than that of pure silica (n_2 = 1.1 x 10^{-15} cm^2/W) [19], matched by a very low linear loss coefficient, negligible nonlinear losses, and a very tight modal confinement afforded by the high index contrast (compared to silica fibers) [20], leading to a nonlinearity parameter (γ) of ~ 220 W^{-1} km^{-1}, roughly 200 times that of standard single mode fibers. Our very low linear losses, much lower than those achievable in silicon or even chalcogenide glass waveguides, allow very long spiral waveguides while maintaining a small device footprint. Moreover, our waveguides are transparent from the near-infrared to the ultra-violet, and hence offer greater potential in terms of a much broader continuum generation than in semiconductors or even chalcogenides. A number of interesting applications have previously been demonstrated in this material platform, including the detection of biomolecules [21], the fabrication of very high order filters (80 dB extinction ratio) [22], as well as low-power nonlinear CW wavelength conversion via four-wave mixing [23,24] and an integrated multi-wavelength hyper-parametric oscillator [25]. Here, we demonstrate SC generation at two wavelengths - 1550 nm and 1290 nm – both of which are in weak dispersion regions, each near a zero-dispersion point (ZDP) characterized by different third order dispersions. At 1550 nm, the normal dispersion regime is at longer wavelengths, whereas at 1290nm it lies at shorter wavelengths. We achieve very broad output spectra at both wavelengths, exceeding 300 nm (at −20 dB) for an excitation centered at 1550nm and more than 350 nm when launching at a central wavelength of 1288 nm. Because the dispersion environment at the two ZDPs is reversed, we observe a significantly different spectral evolution at the two wavelengths, with the spectra at 1288 nm showing clearer soliton fission and Raman self-frequency shifting than the ones observed at 1550 nm.

2. Device

The high-index glass spiral waveguide used in our experiments has a cross-sectional core area of 1.45 x 1.5 μm^2 contained on a footprint area as small as 2.25×2.25 mm^2, as shown in Fig. 1. The core refractive index at 1550nm is 1.7, producing an index contrast with the cladding region (standard fused silica glass) of 17%, in turn allowing for bend radii down to 40μm with negligible loss. Linear propagation losses were estimated to be as small as 0.06dB/cm [19], a result of the advanced CMOS-compatible fabrication process, whereas on-chip coupling losses from single mode fiber pigtails yield a very low loss of < 1.5dB / facet.

The dispersion of these waveguides was previously [23] measured by fitting the resonance wavelengths of a 135μm diameter ring resonator (with the same waveguide cross-section as the spiral reported here) to a 4th order polynomial with the aim to obtain the propagation constant β from 1460nm to 1640nm. The group velocity dispersion was then calculated as $GVD = \beta_2 = d^2\beta/d\omega^2$, where ω is the angular frequency of the propagating light. We found that the waveguide dispersion was not affected by bending, either in the rings or spirals, and this was confirmed numerically using RSoft FemSIM™. The dispersion curves for both the fundamental quasi-TE and quasi-TM modes are depicted by the solids lines in Fig. 2. The zero-dispersion points were obtained at λ = 1560nm and 1595nm for the quasi-TM and quasi-TE modes, respectively, in agreement with the modal analysis of the waveguide. The overall dispersion is dominated by the waveguide geometry – as the material dispersion is very low. As described in [26], we would expect two ZDPs for a step-index waveguide, and our fit predicts another ZDP near 1300 nm, as shown by the dashed lines in Fig. 2. It is important to note that the uncertainty in the projected dispersion outside of the experimental wavelength range of 1460-1640nm is somewhat large due to the strong sensitivity to the fourth order dispersion term, β_4 . By fitting the measured dispersion over this range to a 4th order polynomial, we extract a β_4 of 3.5 x10^{-3} ps^4 km^{-1} [23] with an uncertainty of roughly a factor of 2, and the dispersion near the 1300nm ZDP represents the projection based on this value.

#120004 - $15.00 USD Received 16 Nov 2009; revised 19 Dec 2009; accepted 20 Dec 2009; published 6 Jan 2010

Anomalous dispersion exists between the two ZDPs, which is particularly significant for SC generation. Indeed, as it is described in [1], SC relies on a complicated cascade of many nonlinear interactions, including four-wave mixing. When the phase matching conditions are met, the FWM process can lead to broadband generation of new spectral components, thereby contributing significantly to the overall continuum. It can be shown [24] that the ideal phase matching conditions requires the pump to be placed in a slightly anomalous regime (as the phase matching is a result of the combination of the dispersion and power contributions). Thus, we observed SC spectra when light is launched near each of the predicted ZDPs.

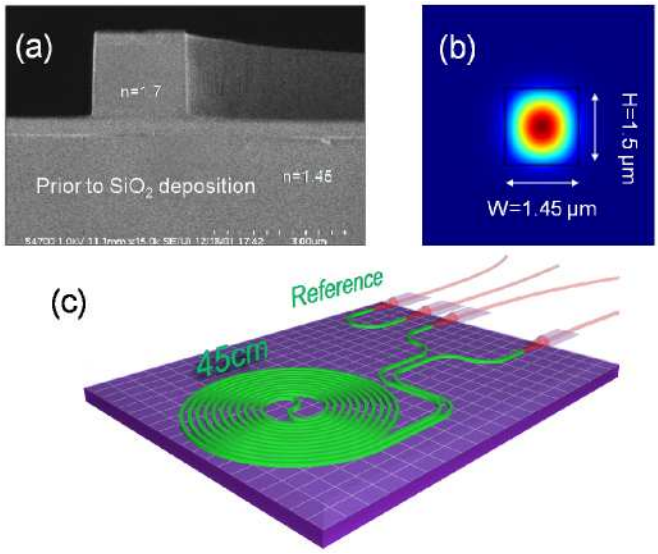

Fig. 1. (a) Scanning electron microscopy image of the cross-section of the high-index waveguide prior to the final deposition of the SiO_2 upper cladding. (b) Theoretical mode profile and (c) Top-down schematic view of the 45cm long spiral waveguide.

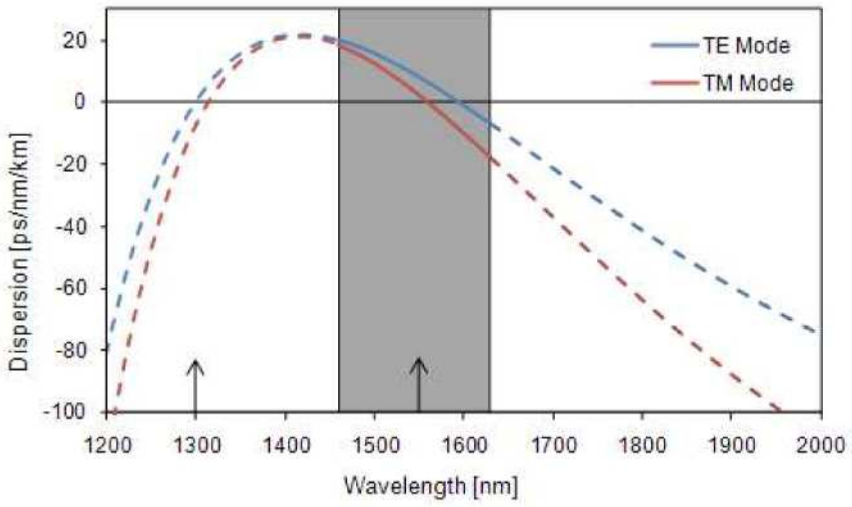

Fig. 2. Dispersion curves for the quasi-TE and quasi-TM modes. The shaded region indicates the experimentally measured wavelength range (solid lines); the dispersion is extrapolated outside this region (dashed lines). The two input pulse wavelengths are illustrated by the vertical arrows.

#120004 - $15.00 USD Received 16 Nov 2009; revised 19 Dec 2009; accepted 20 Dec 2009; published 6 Jan 2010

3. Experiment

The pump source used in our experiments was a Spectra Physics optical parametric oscillator (OPO) generating 100 fs (200fs at 1300nm) long pulses (measured by autocorrelation assuming a Gaussian profile) at a 80 MHz repetition rate. The spectral bandwidth of the pump was 110 nm at 1550 nm (all widths here are measured at −20 dB), and 55 nm at 1288 nm. Polarized pulses from the OPO were passed through a linear variable attenuator and then coupled into a single mode fiber, followed by a reference tap using a 99/1 fiber coupler to allow us to monitor the input power. The output of the waveguide was then directed to an optical spectrum analyzer, and the resulting spectra were recorded for input peak pump powers ranging from 0 to 1.7kW.

4. Results: super-continuum generation at 1550 nm

The experimental output spectra for the first series of measurements with the pump wavelength at 1550 nm are presented in Fig. 3(a) for different input peak powers. At the lowest input powers the pulse undergoes negligible spectral broadening on the scale of the SC spectrum, and so the output spectra reflect the input spectra. As the power is increased, the beam acquires self-phase modulation and the spectrum increases in width with increasing input power [27]. At an input peak power of 1450 W, however, the spectrum widens dramatically towards both the short and long wavelength sides, with the appearance of a new spectral feature near 1450 nm. A further increase in pump power results in a spectral width of more than 300 nm. We observed that some of the more subtle features in the SC spectrum were polarization dependent, but the significant, broad, features – particularly the overall width of the spectrum, were independent of polarization. This is not unexpected since the quasi-TE and quasi-TM polarizations have similar dispersion characteristics on the scale of the SC spectrum (Fig. 2). We verified theoretically that the contribution to spectral broadening from the 1.5m input fiber pigtail was negligible, by including nonlinear effects that are well understood at these power levels in standard SMF [27].

An important part of the evolution of the spectral broadening is soliton fission and dispersive (Cherenkov) radiation. The propagation is expected to be extremely nonlinear with a soliton number greater than 10 (for the highest peak power used in our experiments) [27], whereas the soliton fission length [1] is expected to be on the order of the waveguide length. Simulations were performed in order to verify this, using a generalized slowly-varying envelope approach [27]:

$$\frac{\partial A}{\partial z}+\frac{\alpha}{2}A+i\frac{\beta_2}{2}\frac{\partial^2 A}{\partial T^2}-\frac{\beta_3}{6}\frac{\partial^3 A}{\partial T^3}-i\frac{\beta_4}{24}\frac{\partial^4 A}{\partial T^4}=i\gamma\left(1+\frac{i}{w_0}\frac{\partial}{\partial T}\right)A\int R(T')\left|A(z,T-T')\right|^2 dT',$$

where the electric field of the pulse is defined as $E = A(z,t)\,F(x,y)\exp(-i\omega_0 t + i\beta_0 z)$, and $F(x,y)$ is the transverse modal electromagnetic distribution (found through the use of a finite-element mode solver), $A(z,t)$ is the slowly varying envelope centered at an angular frequency ω_0 and with propagation constant β_0 at ω_0, respectively, α is the linear propagation loss (0.06 dB/cm), $R(T)$ is the Raman response function, T is the time frame moving with the pulse group velocity ($T = t - z/v_g$) and γ is the nonlinear parameter (= 0.22 $m^{-1}W^{-1}$ [16]). The Raman response of our waveguides has yet to be accurately measured, and so we used the Raman response of fused silica as a starting point in our simulations. A Gaussian input envelope, with a small chirp (C = −0.1) to fit both the spectral width and the autocorrelated pulse width, was propagated in the quasi-TE mode in our simulations with β_2 = 10.5 ps^2/km, β_3 = 0.26 ps^3/km, and β_4 = 0.0035 ps^4/km at λ = 1550 nm. This value for β_4 in particular is about a factor of 2 lower than that reported in [25] but is within experimental uncertainty, given the larger error bars for the high order terms.

As it can be seen in Fig. 3(b), the simulations show the general behavior of the experimentally observed spectral broadening. Whereas the features leading to supercontinuum generation were hard to discern experimentally, simulations provided us with

#120004 - $15.00 USD Received 16 Nov 2009; revised 19 Dec 2009; accepted 20 Dec 2009; published 6 Jan 2010

a good understanding of the contributions from the various nonlinear phenomena involved. As the input pulse propagates, it begins to break apart temporally into its constituent fundamental solitons. Initially this is a slow process, resulting in interference fringes as the solitons shift spectrally due to stimulated self-Raman scattering. At an input power near 1450 W, we observe soliton fission, where the rate of this process increases rapidly with increasing input power, and the spectrum becomes much broader. This is accompanied by dispersive wave generation in the normal dispersion regime at longer wavelengths (our measurements were limited by our spectrometer to below 1700nm). Due to the proximity of the ZDP, FWM and modulation instability contribute to the energy transfer at shorter wavelengths. The low-power spectral features observed experimentally between 1350 and 1450 nm (Fig. 3a) were not modeled in our simulations since these were spurious contributions from the OPO not associated with the optical pump pulses. We found, both theoretically and experimentally, that these did not to contribute significantly to the SC process.

5. Results: super-continuum generation at 1288 nm

In contrast to the previous section, when pumping at 1288 nm the normal dispersion regime lies at shorter wavelengths. This situation is in fact typical of most reported demonstrations of SC generation, where many of the phenomena associated with SC generation are observed, such as soliton fission, Raman self-frequency shifting and Cherenkov radiation, and we can see a number of similarly interesting features in the experimental spectra shown in Fig. 4. With a transform limited pulse of 200fs FWHM, and an estimated 50-60% coupling efficiency, the maximum coupled peak power was ~1 kW. Thus, supercontinuum generation is initiated at much lower powers when pumping at 1288nm than when pumping near 1550nm, implying a shorter soliton fission length. This could be due to the waveguide having a larger dispersion than that estimated by extrapolation from the measured data. An easily recognizable feature in the spectrum is soliton self-frequency shift due to Raman scattering, marked as **A**. While it is difficult to observe the dispersive wave on the short wavelength side, the growing spectra at the far side of the 1560 nm ZDP, marked as **B** on Fig. 4, can be interpreted as dispersive radiation, since this grows in the long-wavelength normal dispersion regime. All of these processes contribute to a 350 nm-wide spectrum (at −20 dB) at the maximum power.

Note that we have not shown theoretical results for pumping at 1288nm. The dispersion of the waveguide in this wavelength range was not measured directly but estimated by extrapolating the dispersion measurements at 1460nm-1640nm. We did do simulations to help our own understanding but given the rather large uncertainty due to the sensitivity to higher order dispersion terms (β_4) we did not see the merit in explicitly showing the results.

In terms of the achievable limits of the SC broadened spectra, in both of the experiments (1288nm and 1550nm pump wavelengths) we found that the spectral broadening was limited only by the input power of the source, with both sets of spectra still increasing in width at the highest power levels used in the experiments. On the long wavelength side, the theory predicts spectral broadening substantially beyond the limit of our measurement capability (which was 1700nm, determined by the spectral response of the optical spectrum analyzer (OSA)) - out to near 2000nm - at the higher power levels used in the experiments. Beyond this, it is possible that bend loss and/or material absorption due to phonon resonances could become a limiting factor, but this needs further experimental investigation, and indeed the possibility of achieving mid IR SC generation in these devices is an intriguing possibility. For the short wavelength limit, we also expect, in principle, to be able to achieve novel and useful SC generation even into the visible wavelength range, since, unlike silicon, our waveguides are transparent into the ultra-violet, although the exact nature of the spectral evolution may be complicated by the waveguide becoming multimoded. At the highest power levels, the spectra in Fig. 4 in fact do extend to shorter wavelengths located beyond the wavelength range studied in this work. Investigating the true extent of the possibility for SC generation into the visible wavelength range in this device will be the subject of future work.

#120004 - $15.00 USD Received 16 Nov 2009; revised 19 Dec 2009; accepted 20 Dec 2009; published 6 Jan 2010

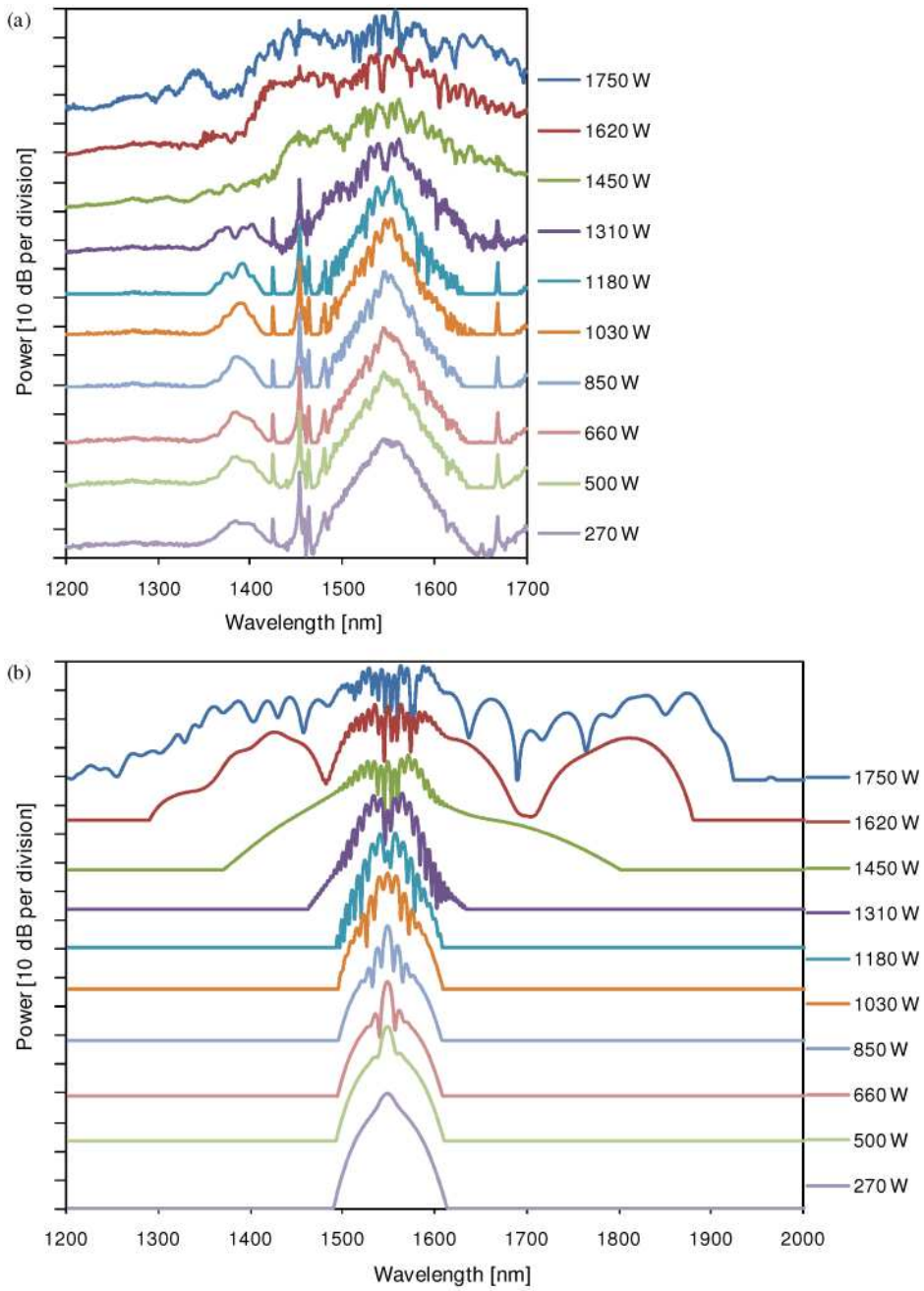

Fig. 3. (a) Experimental and (b) simulated output spectra as a function of coupled peak power for optical pump pulses at 1550 nm. The offset between spectra is proportional to the peak power.

#120004 - $15.00 USD Received 16 Nov 2009; revised 19 Dec 2009; accepted 20 Dec 2009; published 6 Jan 2010

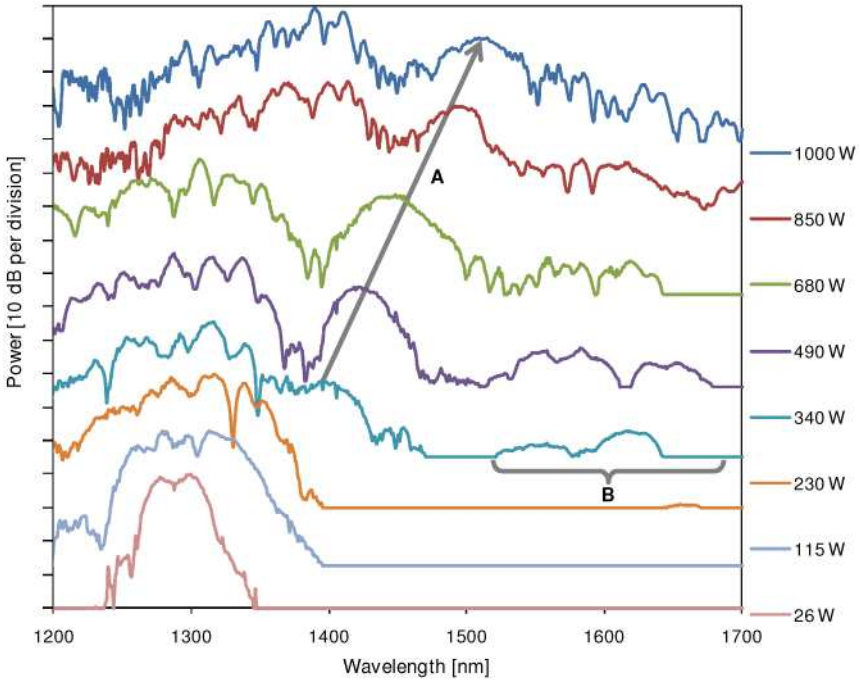

Fig. 4. Experimental output spectra for different input peak powers at 1288 nm. The offset between spectra is proportional to the peak power. (**A**) and (**B**) are features described in the text.

5. Conclusions

We demonstrate SC generation in an integrated, CMOS compatible, 45cm long high index doped silica glass spiral waveguide. We perform SC experiments both in a weak normal and in a weak anomalous dispersion regime, at 1288 nm and 1550 nm respectively. This was found to have a significant impact on the processes contributing to the SC spectra. We obtained a SC spectral width of more than 300 nm at both 1290 nm and 1550 nm. The dispersion of these high-index glass waveguides should allow for SC generation via the injection of relatively high peak power pulses at any wavelength between these ZDPs. Additionally, due to the extended transparency window of our waveguides (reaching visible wavelengths), it should be also possible to achieve SC generation at much shorter wavelengths by engineering the waveguide ZDPs, thus creating visible SC sources.

Acknowledgments

We would like to acknowledge support from the Australian Research Council (ARC) as well as the Natural Sciences and Engineering Research Council of Canada (NSERC) and le Fonds Québécois de la Recherche sur la Nature et les Technologies (FQRNT). MP thanks the Marie Curie People action through project TOBIAS PIOF-GA-2008-221262.

#120004 - $15.00 USD Received 16 Nov 2009; revised 19 Dec 2009; accepted 20 Dec 2009; published 6 Jan 2010